View metadata, citation and similar papers at core.ac.uk

brought to you by CORE

provided by Elsevier - Publisher Connector

Nucl Eng Technol 47 (2015) 416–423

Available online at www.sciencedirect.com

ScienceDirect

journal homepage: http://www.journals.elsevier.com/nuclear-engineering-and-technology/

Original Article

NEW WALL DRAG AND FORM LOSS MODELS FOR ONE-DIMENSIONAL DISPERSED TWO-PHASE FLOW

BYOUNG JAE KIM[*], *SEUNG WOOK LEE*, *and KYUNG DOO KIM*

Thermal-Hydraulic Safety Research Division, Korea Atomic Energy Research Institute, 373-1 Dukjin-dong, Yuseong-gu, Daejeon, 305-701, Republic of Korea

ARTICLE INFO

Article history:
Received 14 May 2014
Received in revised form
17 December 2014
Accepted 1 January 2015
Available online 25 March 2015

Keywords:
Dispersed flow
Form loss
Wall drag

ABSTRACT

It had been disputed how to apply wall drag to the dispersed phase in the framework of the conventional two-fluid model for two-phase flows. Recently, Kim et al. [1] introduced the volume-averaged momentum equation based on the equation of a solid/fluid particle motion. They showed theoretically that for dispersed two-phase flows, the overall two-phase pressure drop by wall friction must be apportioned to each phase, in proportion to each phase fraction. In this study, the validity of the proposed wall drag model is demonstrated though one-dimensional (1D) simulations. In addition, it is shown that the existing form loss model incorrectly predicts the motion of the dispersed phase. A new form loss model is proposed to overcome that problem. The newly proposed form loss model is tested in the region covering the lower plenum and the core in a nuclear power plant. As a result, it is shown that the new models can correctly predict the relative velocity of the dispersed phase to the surrounding fluid velocity in the core with spacer grids.

Copyright © 2015, Published by Elsevier Korea LLC on behalf of Korean Nuclear Society.

1. Introduction

Most thermal-hydraulic codes for nuclear reactor safety analysis are based on two-fluid equations which are obtained by averaging the local instantaneous conservation equations in time, space, or some combination of the two. A key assumption in the standard two-fluid model is that even a dispersed phase is treated as a continuous phase. Therefore, the same averaging process is applied to both phases.

However, that assumption may yield physically-incorrect predictions. One example is the wall drag treatment in the one-dimensional momentum equation for dispersed flows. The methods of determining the wall drag acting on the dispersed phase vary from code to code. The TRACE [2], CATHARE [3], and COBRA-TF [4] do not consider the wall drag force for the dispersed phase based on observations that most droplets/bubbles do not touch the wall. However, this wall drag treatment causes the dispersed phase to be faster than the carrier in a fully-developed horizontal bubbly flow in a pipe with constant area for which two phase velocities are considered to be equal. The local bubble velocity must not exceed the local water velocity in a fully-developed horizontal

* *Corresponding author.*
E-mail address: byoungjae@kaeri.re.kr (B.J. Kim).

This is an Open Access article distributed under the terms of the Creative Commons Attribution Non-Commercial License (http://creativecommons.org/licenses/by-nc/3.0) which permits unrestricted non-commercial use, distribution, and reproduction in any medium, provided the original work is properly cited.

http://dx.doi.org/10.1016/j.net.2015.01.005
1738-5733/Copyright © 2015, Published by Elsevier Korea LLC on behalf of Korean Nuclear Society.

bubbly flow in a pipe with constant area [5,6]. Thus, the wall drag must not be set to zero. The RELAP5 [7] imposes a wall drag force on the bubbles based on the wetted perimeter concept, but the magnitude of the wall drag for the bubbles is even smaller than the physically-correct value.

A question is then raised: what value should we assign to the wall drag force for the dispersed phase? To answer this question, Kim et al. [1] considered different one-dimensional momentum equations based on the equation of a fluid particle motion. They insisted that the magnitude of the wall drag force acting on each phase is the phasic volume fraction multiplied by the overall two-phase pressure drop induced by the interaction between the continuous phase and the wall.

Meanwhile, the form loss designates the loss of momentum due to obstruction or flow separation in nonstraight channels in which the flow area changes abruptly or the pipe is being bent. The existing form loss formulation for a two-phase flow takes the form similar to that used for a single-phase flow. However, such formulation incorrectly predicts the bubble/droplet velocity against the surrounding fluid velocity.

The purpose of this study is to demonstrate the validity of the wall drag model proposed by Kim et al. [1], and to propose a new form loss model for dispersed flows. The concept of the wall drag and form loss are needed only for one-dimensional modeling. Therefore, various one-dimensional simulations were performed using the SPACE code [8] in order to validate the proposed wall drag and form loss models. Fundamental tests were performed in a pipe, contraction, and expansion to validate the new wall drag model. In addition, separate effect tests were carried out in the region covering the lower plenum and the core with grid spacers in a nuclear power reactor, to demonstrate the validity of the new form loss model.

2. Wall drag and form loss for dispersed flow

2.1. Wall drag

This section summarizes the work done by Kim et al. [1]. Unless phase change is considered, the standard volume-averaged momentum equation for phase k can be written as [9]:

$$\alpha_k\rho_k\frac{\partial \mathbf{v}_k}{\partial t}+\alpha_k\rho_k\mathbf{v}_k\cdot\nabla\mathbf{v}_k+\nabla\cdot\left(\alpha_k\boldsymbol{\tau}_k^{\mathrm{Re}}\right) = -\alpha_k\nabla p_k+\nabla\cdot(\alpha_k\boldsymbol{\tau}_k)-\mathbf{f}_{ik}+\alpha_k\rho_k\mathbf{g}, \quad (1)$$

where α_k, ρ_k, $\mathbf{v}_k$, p_k, $\boldsymbol{\tau}_k$, $\mathbf{f}_{ik}$, $\boldsymbol{\tau}_k^{\mathrm{Re}}$, and $\mathbf{g}$ are the volume fraction, density, velocity vector, pressure, viscous stress tensor, interface force, volume-averaged Reynolds stress, and gravitational acceleration, respectively.

Meanwhile, based on the equation of a solid/fluid particle motion [10,11], the volume-averaged momentum equation for an adiabatic dispersed two-phase flow is derived as follows [1,12–14]:

$$\alpha_k\rho_k\frac{\partial \mathbf{v}_k}{\partial t}+\alpha_k\rho_k\mathbf{v}_k\cdot\nabla\mathbf{v}_k+\nabla\cdot\left(\alpha_k\boldsymbol{\tau}_k^{\mathrm{Re}}\right) = -\alpha_k\nabla p_c+\alpha_k\nabla\cdot\boldsymbol{\tau}_c-\mathbf{f}_{ik}+\alpha_k\rho_k\mathbf{g}. \quad (2)$$

Each variable is a volume-averaged quantity. Subscripts d and c are used to indicate the dispersed and continuous phases, respectively.

Comparing Eq. (2) with Eq. (1), one can notice the differences in the second terms on the right-hand sides: (1) α_k is outside the divergence operator with regard to the viscous stress tensor, whereas it is inside the divergence operator in Eq. (1); and (2) the dispersed phase equation is expressed in terms of the pressure and viscous stresses for a continuous phase instead of those for a dispersed phase.

Eq. (2) reduces to the following one-dimensional equation:

$$\alpha_k\rho_k\frac{\partial v_k}{\partial t}+\alpha_k\rho_k v_k\frac{\partial v_k}{\partial x} = -\alpha_k\frac{\partial p}{\partial x}-\alpha_k F_{wt}-f_{ik}+\alpha_k\rho_k g_x. \quad (3)$$

Each of the variables are one-dimensional volume-averaged quantities. The x-direction is the main flow direction. p_c is expressed by p. τ_k^{Re} is neglected because of one-dimensional modeling. f_{ik} is the interface force acting on phase k. In Eq. (2), $\nabla\cdot\tau_c$ is the divergence of the volume-averaged viscous stresses. Thus, it is evaluated as:

$$\nabla\cdot\langle\tau_c\rangle = \langle\nabla\cdot\tau_c\rangle = -F_{wt}, \quad (4)$$

where $\langle\ \rangle$ means the volume averaging over the control volume. F_{wt} is the overall pressure drop induced by the shear of the continuous phase at the wall, which is defined to be a positive value. Consequently, the term $-\alpha_k F_{wt}$ in Eq. (3) indicates that the overall two-phase pressure drop by wall friction is apportioned to each phase in proportion to each phase fraction. This wall drag partition model correctly predicts the relative motion of a bubble/droplet against the surrounding fluid. For a steady horizontal bubbly flow, the bubbles become faster than the water in a contraction whereas the bubble becomes slower in an expansion. For a steady horizontal droplet flow, the droplet is slower than the gas in a contraction whereas the droplet is faster in an expansion. These behaviors are attributed to the fact that compared with the lighter fluid, the heavier fluid slowly accelerates or decelerates in response to the changes in circumstances. Of course, two velocities become equal for a fully-developed flow in a pipe with constant area. A detailed theoretical discussion is described in Kim et al. [1].

2.2. Form loss

The form loss designates the loss of momentum due to an obstruction or flow separation in nonstraight channels in which the flow area changes abruptly or the pipe is being bent. The contribution of the form loss is usually added to the one-dimensional momentum equation as follows:

$$\alpha_k\rho_k\frac{\partial v_k}{\partial t}+\alpha_k\rho_k v_k\frac{\partial v_k}{\partial x} = -\alpha_k\frac{\partial p}{\partial x}-\alpha_k F_{wt}-f_{ik}+\alpha_k\rho_k g_x -\frac{K_k}{2L}\alpha_k\rho_k\left|v_k\right|v_k. \quad (5)$$

The last term accounts for the form loss, where K_k is the form loss factor for phase k in the channel length L. Consider a fully-developed horizontal bubbly flow at the region in which K_k has a nonzero value whereas the flow area remains unchanged. This situation may be encountered at the bending

region of a pipe. In this case, Eq. (5) can be written for each phase as follows:

$$0 = -\alpha_d \frac{\partial p}{\partial x} - \alpha_d F_{wt} - f_{id} - \frac{K_d}{2L}\alpha_d \rho_d \left|v_d\right| v_d \tag{6}$$

$$0 = -\alpha_c \frac{\partial p}{\partial x} - \alpha_c F_{wt} - f_{ic} - \frac{K_c}{2L}\alpha_c \rho_c \left|v_c\right| v_c \tag{7}$$

The pressure drop results not only from wall friction, but also form loss. The linear relation is assumed.

$$-\frac{\partial p}{\partial x} = \left(-\frac{\partial p}{\partial x}\right)_w + \left(-\frac{\partial p}{\partial x}\right)_K \tag{8}$$

The first and second terms in the right-hand side are the contributions of wall friction and form loss, respectively. Substituting Eq. (8) into Eqs. (6) and (7), and using the relations $(-\partial p/\partial x)_w = F_{wt}$ and $f_{ic} = -f_{id}$, we can have:

$$0 = \alpha_d \left(-\frac{\partial p}{\partial x}\right)_K - f_{id} - \frac{K_d}{2L}\alpha_d \rho_d \left|v_d\right| v_d \tag{9}$$

$$0 = \alpha_c \left(-\frac{\partial p}{\partial x}\right)_K + f_{id} - \frac{K_c}{2L}\alpha_c \rho_c \left|v_c\right| v_c \tag{10}$$

If we multiply the first equation by α_c and the second by α_d and subtract the first from the second, the pressure term is eliminated. The resultant equation is arranged to give:

$$f_{id} = \frac{\alpha_c \alpha_d}{2L}\left(K_c \rho_c |v_c| v_c - K_d \rho_d |v_d| v_d\right) \approx \frac{\alpha_c \alpha_d}{2L} K_c \rho_c \left|v_c\right| v_c \tag{11}$$

The last approximation is because the bubble density is much smaller than the water density. Given the positive direction of the continuous phase velocity in Eq. (11), f_{id} has a positive value. Thus, by definition,

$$f_{id} = C_i \left|v_d - v_c\right| (v_d - v_c) > 0 \tag{12}$$

where C_i is the interface drag coefficient and has a positive value. Eq. (12) indicates that the bubbles become faster than the water. This prediction seems physically incorrect. As the flow area remains unchanged, the averaged water velocity would not accelerate or decelerate. The motion of a bubble is driven by the water, so the dispersed phase velocity would also not change. In a similar manner, it can be shown that the existing form loss model predicts that the droplet becomes slower than the gas in a fully-developed droplet flow in a straight pipe. In the case of an abrupt area change, however, because the acceleration/deceleration rate of the dispersed phase differs from that of the continuous phase, the relative velocity between the two phases varies along the channel.

A new form loss formulation is now proposed to make two velocities equalize. The overall momentum loss for the two-phase mixture due to the form loss, F_{loss}, is first computed using the form loss factor for a continuous phase.

$$F_{loss} = -\frac{K_c}{2L}\alpha_c \rho_c \left|v_c\right| v_c. \tag{13}$$

The total momentum loss may be calculated using a different method. F_{loss} is then apportioned to each phase in proportion to each phasic fraction. Instead of Eqs. (9) and (10), we write as follows:

$$0 = \alpha_d \left(-\frac{\partial p}{\partial x}\right)_K - f_{id} - \alpha_d F_{loss}, \tag{14}$$

$$0 = \alpha_c \left(-\frac{\partial p}{\partial x}\right)_K + f_{id} - \alpha_c F_{loss}. \tag{15}$$

The pressure gradient term $(-\partial p/\partial x)_K$ naturally equals F_{loss}. Thus, the first and third terms on the right-hand sides in Eqs. (14) and (15) sum to zero. As a result, two velocities become identical owing to the fact that $f_{id} = 0$. It is of interest to note that this partitioning approach is consistent with the wall drag partitioning described in the preceding section. Note that the form loss is merely a different expression of the wall drag.

The effects of the new wall drag and form loss models are summarized in Table 1. The existing model in the wall drag column refers to the cases in which the wall drag term is set to zero in the momentum equation for the dispersed phase. Although the existing model predicts that the dispersed phase is faster than the continuous phase in a fully-developed horizontal flow, the new wall drag model makes two velocities equalize. As to the form loss, the existing model corresponds to the formulation given in the last term of Eq. (5). Compared with the existing model, the new form loss model decreases the bubble velocity but increases the droplet velocity. In general, the pressure drop by wall friction is more considerable in a bubbly flow than in a gas flow. Therefore, the new models have more pronounced effects on the motion of the bubble rather than the droplet. The wall temperatures of the fuel rods predicted by the new wall and form loss models are higher than those predicted by the existing models, as the heat transfer between the fuel rods and the coolant deteriorates when the void fraction increases. This means that the existing models are less conservative than the newly proposed models from the point of view of safety analysis.

3. Results and discussion

3.1. *Demonstration of the new wall drag partition model*

Fundamental tests were conducted to demonstrate the validity of the new wall drag model for dispersed flows. One-dimensional simulations were performed using the SPACE code [8]. Three basic test channels are depicted in Fig. 1: straight pipe, contraction, and expansion. Geometrical

Table 1 – Predictions of fluid velocities for horizontal fully-developed dispersed flows in a pipe with constant area.

	Wall drag model		Form loss model		Combined effects of the new models
	Existing	New	Existing	New	
Bubble	$v_d > v_c$	$v_d = v_c$	$v_d > v_c$	$v_d = v_c$	Considerable decrease in the bubble velocity
Droplet	$v_d > v_c$	$v_d = v_c$	$v_d < v_c$	$v_d = v_c$	Slight decrease/increase in the droplet velocity

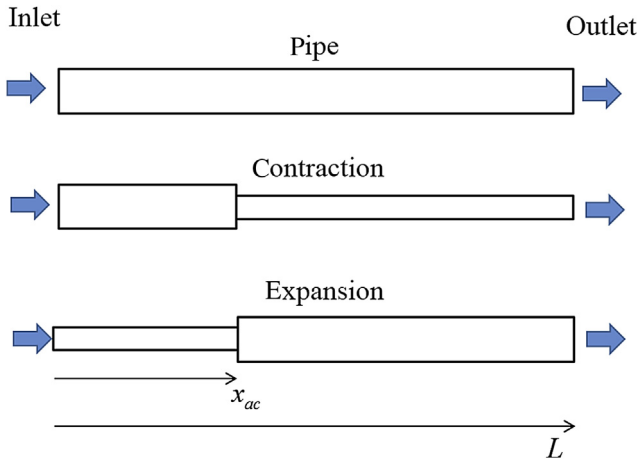

Fig. 1 – Test channels for the validation of the wall drag model.

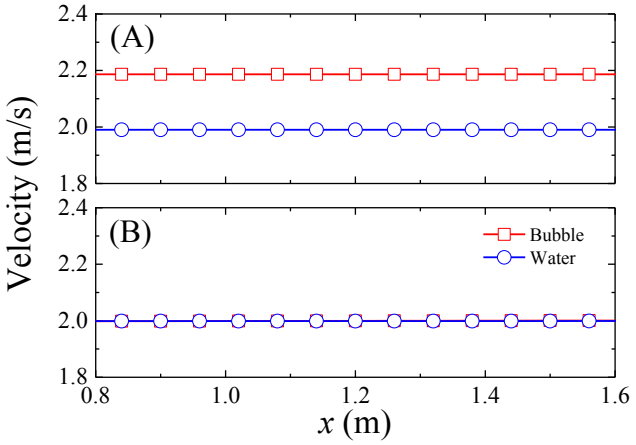

Fig. 2 – Bubbly flow in the pipe: (A) existing model and (B) new model.

dimensions are given in Table 2, where L, A, and x_{ac} are the total flow length, flow area, and the location at which the flow area changes abruptly. A flow area of 1.50×10^{-4} m^2 corresponds to that of a typical subchannel. To isolate the problem from any other effects, phase change, horizontal stratification, and droplet entrainment/deposition were not allowed to occur.

The test pressure was the saturation pressure of 10 bar. For bubbly flows, the void fraction and fluid velocities were set to 0.05 m/s and 2.0 m/s at the inlet, respectively. For droplet flows, the droplet fraction and fluid velocities were set to 0.02 m/s and 20.0 m/s, respectively. The form loss factor was set to zero at $x = x_{ac}$ to examine the wall drag effect. A longer channel length is required for a droplet flow to be fully developed. The models of the interface drag and the overall two-phase pressure drop by wall friction are described in Appendix 1.

Figs. 2–4 show the fluid velocities in bubbly flows. One can see in Fig. 2 that the bubble is faster than the water when the wall drag is applied only to the water (existing model). This prediction is physically incorrect. However, the bubble velocity becomes equal to the water velocity when the overall pressure drop by wall friction is apportioned to each phase in proportion to each phase fraction (new model). The fluid velocities in the contraction and expansion are shown in Figs. 3 and 4, respectively. When the wall drag is applied only to the water, the bubble becomes faster than the water in the upstream or downstream flow. If the wall drag is corrected, the relative velocity of the bubble to the water is predicted correctly. Although the bubble is faster than the water in the contraction region, the bubble is slower in the expansion region. The relative velocity of the bubble to the water is significantly affected by the magnitude of the interface drag. The less the interface drag is, the more apparent the relative velocity becomes. The bubble diameters in the tests are estimated as 2.9 mm by Hibiki's correlation described in Appendix 1.

Figs. 5–7 show the fluid velocities for droplet flows. As expected, a longer channel length is needed for a droplet flow to be fully developed than for a bubbly flow. For the pipe flow in Fig. 5, the existing wall drag model shows the droplet velocity to be slightly higher than the gas velocity. However, this incorrect prediction is solved by the new wall drag model. In Fig. 5, the fluid velocities increase continuously in the downstream flow because the gas density decreases. It is shown in Figs. 6 and 7 that the droplet phase is slower than the gas phase in the contraction region, and the droplet is faster than the gas in the expansion region. The relative motion of the droplet against the gas is less apparent than the relative motion of the bubble to the water (Figs. 2–4). The reasons are the increased interface drag by small droplet diameter (200 μm) and the small pressure drop by wall friction. As the interface

Table 2 – Geometrical dimensions of test channels shown in Fig. 1.

Flow	Channel	A ($\times 10^{-4}$ m^2)	L (m)	x_{ac} (m)
Bubbly flow	Pipe	1.23	5.94	–
	Contraction	1.50→1.23	5.94	1.2
	Expansion	1.23→1.50	5.94	1.2
Droplet flow	Pipe	1.23	29.4	–
	Contraction	1.50→1.23	29.4	11.76
	Expansion	1.23→1.50	29.4	11.76

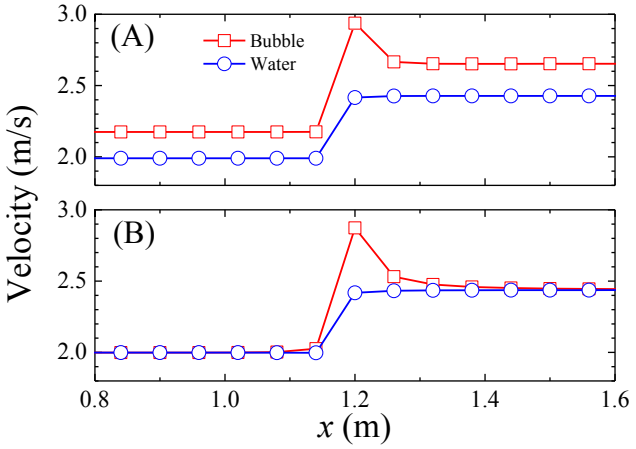

Fig. 3 – Bubbly flow in the contraction: (A) existing model and (B) new model.

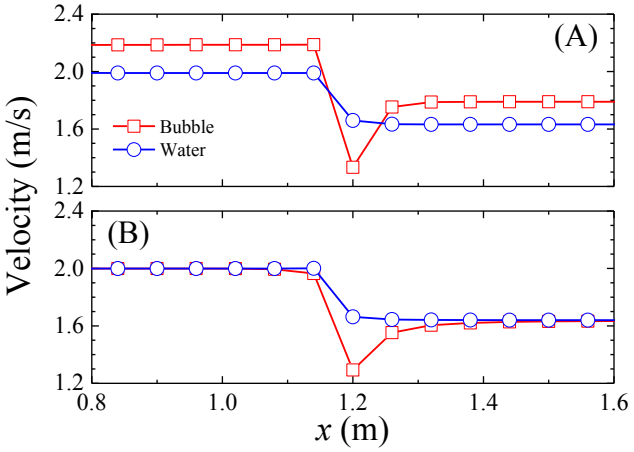

Fig. 4 – Bubbly flow in the expansion: (A) existing model and (B) new model.

drag increases, the droplet follows the gas more faithfully. As the pressure drop is small, the wall drag effect becomes less important than the interface drag.

The relative motion of the bubble/droplet to the surrounding fluid in the contraction/expansion can be explained by the fact that the lighter fluid accelerates or decelerates more quickly than the heaver fluid. Therefore, the bubbles are faster than the water in the contraction region, but slower in the expansion region. As to the droplet, it is slower than the gas in the contraction, but faster in the expansion region. The new wall drag model can predict these behaviors, as shown in Figs. 3, 4, 6, and 7. The RELAP5 code imposes the wall drag on the dispersed phase, based on the wetted fraction concept. Although the results are not provided here, they are nearly the same as those seen when the wall drag is not imposed on the dispersed phase. The existing thermal-hydraulic codes calculate incorrectly the magnitude of the wall drag for the dispersed phase.

3.2. *Demonstration of the new form loss model*

The next tests focus on the flow phenomena in the region from the lower plenum to the core in a nuclear power reactor.

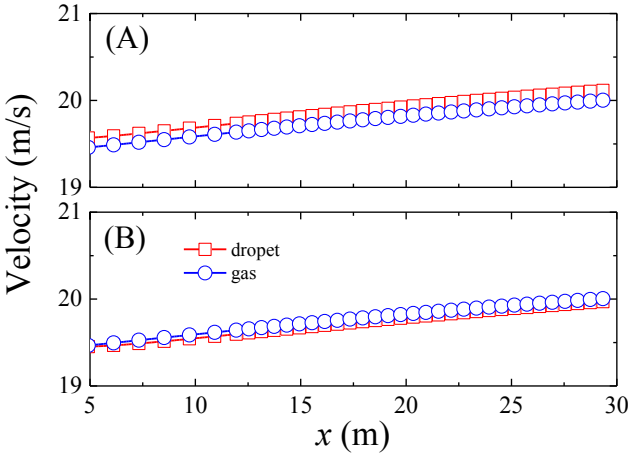

Fig. 5 – Droplet flow in the pipe: (A) existing model and (B) new model.

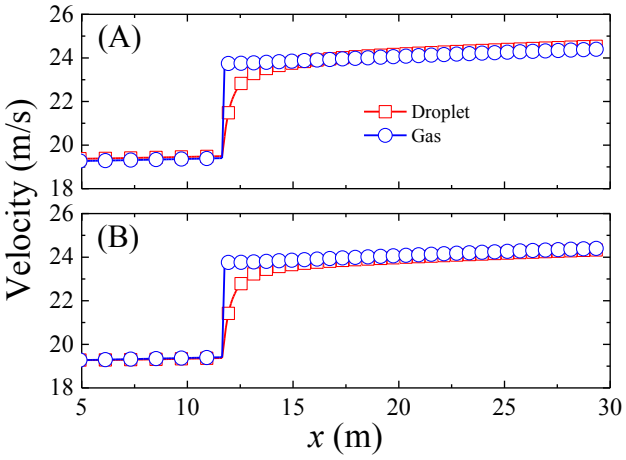

Fig. 6 – Droplet flow in the contraction: (A) existing model and (B) new model.

A schematic diagram is shown in Fig. 8. The lower plenum and the core channel were modelled using pipe components. Heat structures for the fuel rods were not considered because the present study deals with hydrodynamic aspects. Tests were performed not only for a vertical channel, but also a horizontal channel, to see the relative importance of the wall drag and form loss to the gravity. The dimensions used are those for a typical rod bundle geometry of a nuclear power plant. The lower plenum length was intentionally elongated for the flow to be fully developed at the entrance into the core.

The tests were conducted at a saturation pressure of 70 bar. The void fraction and fluid velocities were set to 0.05 m/s and 1.0 m/s, respectively, at the inlet. Grid spacers were realized by imposing a nonzero form loss factor ($K = 1.22$) at nine locations throughout the core. The flow area does not change in the core. For the horizontal tests, the flow was forced to be bubbly by prohibiting horizontal stratification. Phase change was not allowed to occur.

Figs. 9 and 10 show the horizontal flow results. The bubble diameter is estimated as 1.1 mm in the core. Hibiki's correlation, however, tends to predicts a considerably large bubble

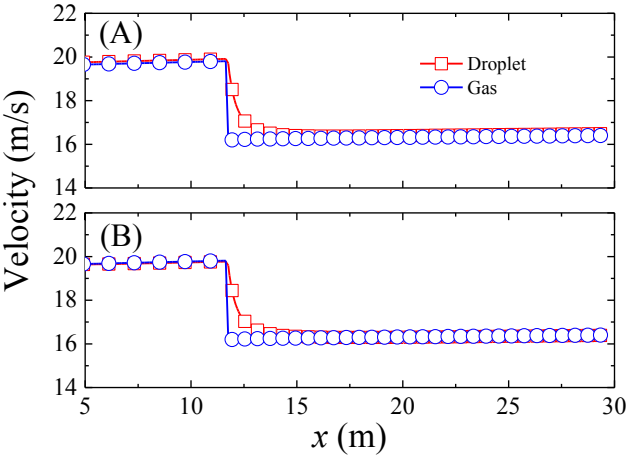

Fig. 7 – Droplet flow in the expansion: (A) existing model and (B) new model.

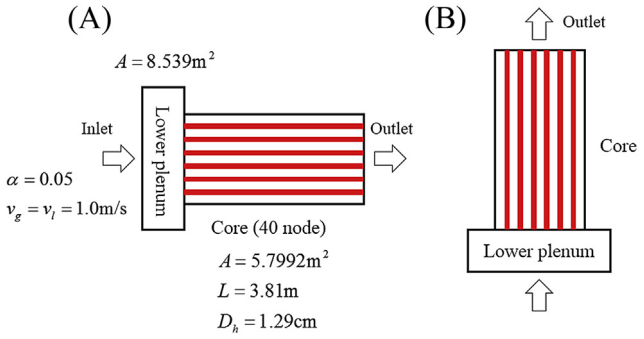

Fig. 8 – Test channels for the validation of the form loss model: (A) horizontal flow and (B) vertical flow.

diameter in the lower plenum, and thus, bubble diameter is set to be 2.0 mm in the lower plenum region. In Figs. 9 and 10, the bubble velocity is nearly the same as the water velocity in the lower plenum region ($x < 0$) for both the existing and new models. The reason is that the pressure drop by wall friction is not very high in that region with a large hydraulic diameter. Therefore, the wall drag model does not affect the results. However, the relative velocity of the bubble to the water becomes apparent in the core region where the pressure drop due to wall friction is considerably high. One can see that regardless of the wall drag model, the bubble velocity shows spikes at the grid spacer locations when the existing form loss model is used (Fig. 9). As mentioned previously, this prediction is incorrect. As the flow area is uniform, the relative velocity of the bubble to the water should not change. Fig. 10 shows the prediction result when the new wall drag and form loss models are used. The bubble diameter is the same as that for horizontal flows. The bubble is faster than the water for some distance from $x = 0$, but the two velocities soon equalize in the core region. This prediction is correct and demonstrates the validity of the proposed wall and form loss models.

The numerical simulations were carried out for vertical flows in the geometry shown in Fig. 8B. The results are shown in Figs. 11 and 12. On the whole, the bubble velocity is higher

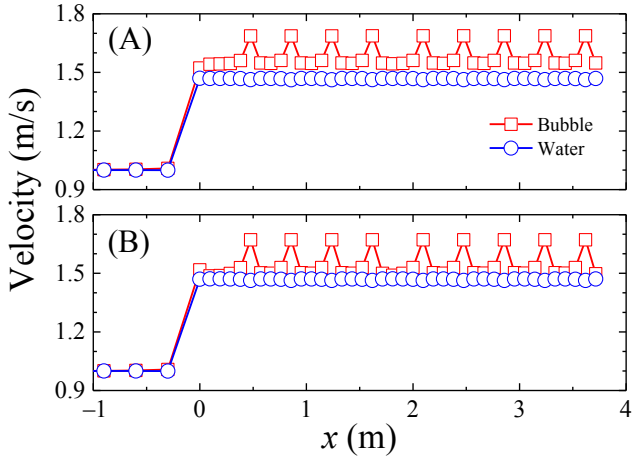

Fig. 9 – Horizontal bubbly flow for Fig. 8A when the existing form loss model is used: (A) existing wall drag model and (B) new wall drag model.

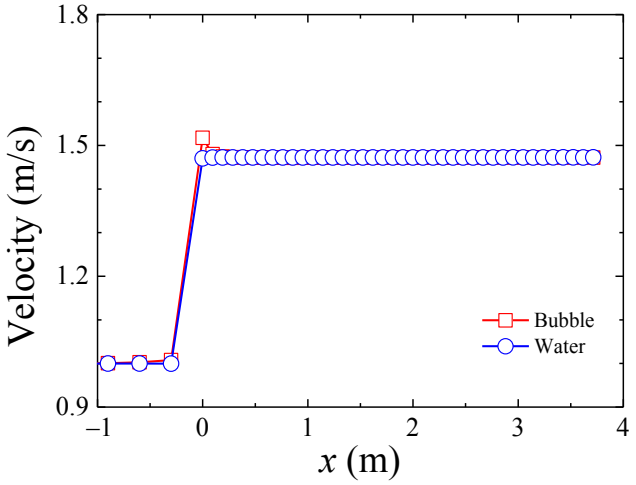

Fig. 10 – Horizontal bubbly flow for Fig. 8A when the new wall and form loss models are used.

than the water velocity due to the buoyancy force. Fig. 11 shows that the two wall drag models yield nearly the same results because the magnitude of wall drag forces is smaller than the buoyancy force. For bubbly flow, the pressure drop by wall friction is approximately proportional to the square of water velocity. Therefore, the wall drag effect can be compared with the gravity effect when the water velocity is increased further. This situation may occur in the core at the initial state of large break loss-of-coolant accident. Fig. 11 shows that there are peaks in the bubble velocity at the grid spacer locations when the existing form loss model is used. Fig. 12 shows the result when the new wall drag and form loss models are used. It is clearly shown that the new models also work well in vertical flows. The effect of the present form loss model will be more apparent if the form loss factor is increased further.

3.3. *Concluding remarks*

This study can be summarized as follows: (1) one-dimensional simulations in a pipe, contraction, and expansion successfully

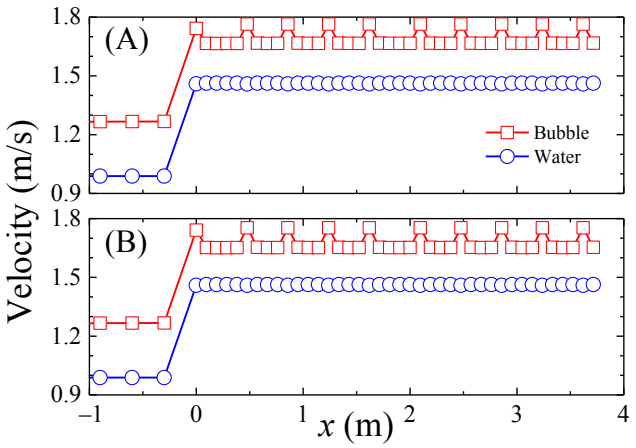

Fig. 11 – Vertical bubbly flow for Fig. 8B when the existing form loss model is used: (A) existing wall drag model and (B) new wall drag model.

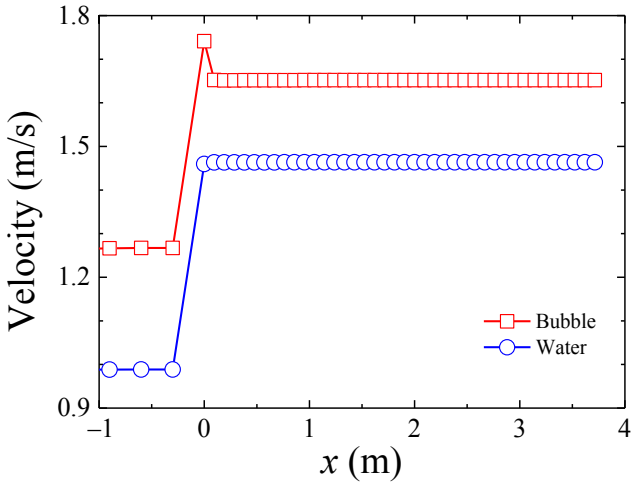

Fig. 12 – Vertical bubbly flow for Fig. 8B when the new wall and form loss models are used.

demonstrated the validity of the proposed wall drag partitioning model for dispersed flows; (2) a new form loss formulation was proposed. The overall momentum loss was apportioned to each phase in proportion to each phase fraction. This partition is consistent with the wall drag partition; and (3) the proposed wall drag and form loss models can correctly predict the dispersed phase velocity in the core with spacer grids. The proposed models are more conservative from a safety analysis point of view, because the wall temperatures of the fuel rods predicted by the proposed models are higher than those predicted by the existing models.

Conflicts of interest

All contributing authors declare no conflicts of interest.

Acknowledgments

This work was supported by the Nuclear Power Technology Development Program of the Korea Institute of Energy Technology Evaluation and Planning (KETEP) grant funded by the Korea Government Ministry of Knowledge Economy (MKE); and by the Nuclear Safety Research Center Program of the KORSAFe grant (Grant Code 1305011) funded by the Nuclear Safety and Security Commission of the Korean government.

Appendix 1. Models for the interface drag and the pressure drop by wall friction.

The interface drag acting on the dispersed phase f_{id} is computed:

$$f_{id} = \frac{1}{8}\rho_c C_D a_i \left|v_d - v_c\right|(v_d - v_c), \tag{A.1}$$

$$C_D = \frac{24}{\mathrm{Re}_d}(1.0 + 0.1\mathrm{Re}_d^{0.75}), \tag{A.2}$$

$$\mathrm{Re}_d = \frac{\rho_c d_d |v_d - v_c|}{\mu_c/(1-\alpha_d)}, \tag{A.3}$$

where a_i, d_d, and μ_c are the interfacial area density, the disperse phase (bubble or droplet) diameter, and the continuous phase viscosity, respectively [15]. Subscripts d and c represent the dispersed and continuous phases, respectively. The bubbles are assumed to be spherical. The interfacial area density is given by:

$$a_i = \frac{6\alpha_d}{d_d}. \tag{A.4}$$

The bubble diameter is computed by [16]:

$$d_d = 1.99\left(\frac{l}{D_H}\right)^{-0.335}\left(\frac{\varepsilon^{1/3}l^{4/3}}{\mu_f/\rho_f}\right)^{-0.239} l, \tag{A.5}$$

where $l = (\sigma/(\rho_c - \rho_d)/g)^{1/2}$ is the capillary length and D_H is the channel hydraulic diameter. In bubbly flows, subscripts d and c indicate bubble $(d = g)$ and the surrounding liquid $(c = f)$, respectively. The energy dissipation rate per unit mass ε in Eq. (A.5) is calculated as:

$$\varepsilon = g j_g \exp(-A\mathrm{Re}_f) + \frac{j}{\rho_m}\left(-\frac{dp}{dx}\right)_w (1 - \exp(-A\mathrm{Re}_f)), \tag{A.6}$$

where $j_g = \alpha_g v_g$, $j = \alpha_g v_g + \alpha_f v_f$, $\rho_m = \alpha_g\rho_g + \alpha_f\rho_f$, $A = 0.0005839$, and $\mathrm{Re}_f = \alpha_f\rho_f v_f D_H/\mu_f$. $(-dp/dx)_w$ is the overall two-phase pressure drop by wall friction. Hibiki's correlation is valid for $D_H < 0.35$ m. As to the droplet diameter, it is set to $d_d = 200$ μm for all simulation runs.

The overall two-phase pressure drop by wall friction is obtained based on the two-phase multiplier approach:

$$\left(-\frac{dp}{dx}\right)_w = \left(-\frac{dp}{dx}\right)_g + C\left[\left(-\frac{dp}{dx}\right)_g\left(-\frac{dp}{dx}\right)_f\right]^{1/2} + \left(-\frac{dp}{dx}\right)_f, \tag{A.7}$$

where $(-dp/dx)_g$ and $(-dp/dx)_f$ are the gas phase-alone and liquid phase-alone wall friction pressure drops, respectively, and C is the correlation coefficient. The k phase-alone wall friction pressure drop is calculated by:

$$\left(-\frac{dp}{dx}\right)_k = \frac{2f_k(\alpha_k\rho_k v_k)^2}{D_H\rho_k}. \tag{A.8}$$

The fanning friction factor f_k is calculated by the Churchill [17] correlation:

$$f_k = 2\left((8/\mathrm{Re}_k)^{12} + 1/(a+b)^{3/2}\right)^{1/12}, \tag{A.9}$$

where

$$a = \left[2.475\ln\left(\frac{1}{(7/\mathrm{Re}_k)^{0.9} + 0.27\min[0.02, \max[10^{-9}, e/D_H]]}\right)\right]^{16},$$

$$b = (37530/\mathrm{Re}_k)^{16},$$

$$\mathrm{Re}_k = \alpha_k\rho_k v_k D_H/\mu_k,$$

e: channel roughness (m).

Finally, coefficient C in Eq. (A.7) is computed by the Claxton et al. [18] correlation:

$$C = \max[2, -2 + f1 \cdot T1], \tag{A.10}$$

where

$$f1 = 28 - 0.3G_m^{1/2},$$

$$T1 = \exp\left(-\frac{(\log_{10}\Lambda + 2.5)^2}{2.4 - 10^{-4}G_m} \right),$$

$$\Lambda = \frac{\rho_g}{\rho_f}\left(\frac{\mu_f}{\mu_g}\right)^{0.2},$$

$$G_m = \alpha_g \rho_g v_g + \alpha_f \rho_f v_f.$$

REFERENCES

[1] B.J. Kim, J. Kim, K.D. Kim, On the wall drag term in the averaged momentum equation for dispersed flows, Nucl. Sci. Eng. 178 (2014) 225–239.

[2] USNRC, Trace V5.840 Theory Manual: Fields Equations, Solution Methods, and Physical Models, U.S. Nuclear Regulatory Commission, 2013.

[3] D. Bestion, The physical closure laws in the cathare code, Nucl. Eng. Des. 124 (1990) 229–245.

[4] C.Y. Paik, L.E. Hochreiter, J.M. Kelly, R.J. Kohrt, Analysis of Flecht-Seaset 163-Rod Blocked Bundle Data Using Cobra-Tf, NUREG/CR-4166, EPRI-NP-4111, WCAP-10375, Westinghouse Electric Corporation, 1985.

[5] G. Kocamustafaogullari, Z. Wang, An experimental study on local interfacial parameters in a horizontal bubbly two-phase flow, Int. J. Multiphase Flow 17 (1991) 553–572.

[6] G. Kocamustafaogullari, W.D. Huang, Internal structure and interfacial velocity development for bubbly two-phase flow, Nucl. Eng. Des. 151 (1994) 79–101.

[7] USNRC, Relap5/Mod3.3 Code Manual Vol. IV: Models and Correlations, NUREG/CR-5535/Rev P4-Vol IV, Nuclear Regulatory Commission, 2010.

[8] S.J. Ha, C.E. Park, K.D. Kim, C.H. Ban, Development of the space code for nuclear power plants, Nucl. Eng. Technol. 43 (2011) 45–62.

[9] D.A. Drew, Mathematical modeling of two-phase flow, Ann. Rev. Fluid Mech. 15 (1983) 261–291.

[10] M.R. Maxey, J.J. Riley, Equation of motion for a small rigid sphere in a nonuniform flow, Phys. Fluids 26 (1983) 883–889.

[11] P.M. Lovalenti, J.F. Brady, The force on a bubble, drop, or particle in arbitrary time-dependent motion at small Reynolds number, Phys. Fluids 5 (1993) 2104–2116.

[12] T.B. Anderson, R. Jackson, Fluid mechanical description of fluidized beds: equations of motion, Ind. Eng. Chem. Fundamen. 6 (1967) 527–539.

[13] A. Prosperetti, A.V. Jones, Pressure forces in disperse two-phase flow, Int. J. Multiphas. Flow. 10 (1984) 425–440.

[14] C. Crowe, J.D. Schwarzkopf, M. Sommerfeld, Y. Tsuji, Multiphase Flows with Droplets and Particles, second ed., CRC Press, New York, 2011.

[15] M. Ishii, T.C. Chawla, Local Drag Laws in Dispersed Two-phase Flow, NUREG/CR-1230, ANL-79–105, Argonne National Laboratory, 1979.

[16] T. Hibiki, M. Ishii, Interfacial area concentration of bubbly flow systems, Chem. Eng. Sci. 57 (2002) 3967–3977.

[17] S.W. Churchill, Friction-factor equation spans all fluid-flow regimes, Chem. Eng. 84 (1977) 91–92.

[18] K.T. Claxton, J.G. Collier, J.A. Ward, H.T.F.S. Correlations for Two-phase Pressure Drop and Void Fraction in Tubes, AERE-R7162, 1972.